

Absorption/Transmission Measurements of PSAP Particle-Laden Filters from the Biomass Burning Observation Project (BBOP) Field Campaign

Cary Presser,^{*‡} Ashot Nazarian,^{*} Joseph M. Conny,^{*} Duli Chand,[†] Arthur Sedlacek,[§]

and John M. Hubbe[†]

^{*}National Institute of Standards and Technology

[†]Pacific Northwest National Laboratory

[§]Brookhaven National Laboratory

ABSTRACT

Absorptivity measurements with a laser-heating approach, referred to as the laser-driven thermal reactor (LDTR), were carried out in the infrared and applied at ambient (laboratory) non-reacting conditions to particle-laden filters from a three-wavelength (visible) particle/soot absorption photometer (PSAP). The particles were obtained during the Biomass Burning Observation Project (BBOP) field campaign. The focus of this study was to determine the particle absorption coefficient from field-campaign filter samples using the LDTR approach, and compare results with other commercially available instrumentation (in this case with the PSAP, which has been compared with numerous other optical techniques). Advantages of the LDTR approach include 1) direct estimation of material absorption from temperature measurements (as opposed to resolving the difference between the measured reflection/scattering and transmission), 2) information on the filter optical properties, and 3) identification of the filter material effects on particle absorption (e.g., leading to particle absorption enhancement or shadowing). For measurements carried out under ambient conditions, the particle absorptivity is obtained with a thermocouple placed flush with the filter back surface and the laser probe beam impinging normal to the filter particle-laden surface. Thus, in principle one can employ a simple experimental arrangement to measure simultaneously both the transmissivity and absorptivity (at different discrete wavelengths) and ascertain the particle absorption coefficient. For this investigation, LDTR measurements were carried out with PSAP filters (pairs with both blank and exposed filters) from eight different days during the campaign, having relatively light but different particle loadings. The observed particles coating the filters were found to be carbonaceous (having broadband absorption characteristics). The LDTR absorption coefficient compared well with results from the PSAP. The analysis was also expanded to account for the filter fiber scattering on particle absorption in assessing particle absorption enhancement and shadowing effects. The results indicated that absorption enhancement effects were significant, and diminished with increased filter particle loading.

Key Words: absorption coefficient; Biomass Burning Observation Project; laser-driven thermal reactor; particle/soot absorption photometer; particle absorption; particle-laden filters

‡Corresponding Author

Cary Presser
Research Engineer
Chemical Process Measurements Group
Chemical Sciences Division
Material Measurement Laboratory

Mailing Address:

National Institute of Standards and Technology
Bldg. 221, Rm. B310
100 Bureau Dr., Stop 8320
Gaithersburg, MD 20899-8320

Contact:

301-975-2612 (tel)
cpresser@nist.gov (email)

1. BACKGROUND – BBOP FIELD CAMPAIGN

Aerosols from biomass burning are recognized to perturb Earth's climate through direct effects (both scattering and absorption of incoming radiation), semi-direct effects (evaporation of cloud drops due to absorbing aerosols), and indirect effects (by influencing cloud formation and precipitation, e.g., Kaufman et al. [2002], Andrea and Rosenfeld [2008]). Biomass burning is an important aerosol source, providing an estimated 50 % of anthropogenic-generated fine carbonaceous particles [Bond et al. 2004], Andrea and Rosenfeld 2008]. Organic carbon is a major component of biomass-burn aerosol [de Gouw and Jimenez 2009], having a significant spectral dependence that if underestimated in models can influence estimation of the aerosol radiative forcing [Kirchstetter et al. 2004]. Data from the IMPROVE (Interagency Monitoring of Protected Visual Environments [EPA 2012]) network have shown that in large sections of the US, aerosols from fires (defined to include agricultural burns and forest fires, both prescribed and wild) comprise a major fraction of the aerosol mass. Their year-to-year variability dominates the overall variability of aerosol loading and radiative forcing [Park et al. 2007].

Sampling biomass burning aerosols presents unique challenges. In addition to the sporadic nature of wildfires and the relative short lifetime of prescribed burns, fires may lack spatial homogeneity. Part or all of a fire can contain a dynamic mix of flaming and smoldering combustion, each of which produces aerosol with different optical properties evolving over a variety of time scales [Vakkari et al. 2014]. Particle emissions from these fires consist, in part, of fractal-like soot (e.g., Martins et al. [1998]), tar balls (nearly spherical amorphous particles containing organic brown carbon, primarily absorbing at the ultraviolet/visible wavelengths) (e.g., Tóth et al. [2014], Adachi and Buseck [2011], Chakrabarty et al. [2010], Pósfai et al. [2004]), and refractory black carbon (e.g., Sedlacek et al. [2015]). Combustion from flames is characterized by the production of black carbon, while smoldering combustion is dominated by the production of organic brown carbon [Hoffer et al. 2006]. Black and brown carbon are optically defined as light absorbing compounds, but the imaginary part of the refractive index for black carbon is essentially independent of wavelength (and absorption cross section inversely proportional to wavelength) [Lack and Cappa 2010], while the refractive index imaginary part for brown carbon decreases with increasing wavelength [Jacobson 2012].

Field campaigns in northern temperate latitudes have been overwhelmingly devoted to other aerosol sources, in spite of biomass burning producing about one-third of the fine particles (PM_{2.5}) in the US [Kleinman and Sedlacek 2013]. Many large field campaigns have focused on biomass burning in tropical regions, while only a few smaller-scale, aircraft-based field campaigns have focused on fire emissions in the US (e.g., Yokelson et al. [1999], Goode et al. [2000], Burling et al. [2011]). The relatively infrequent occurrence of fires in the US, compared to the Amazon, Africa, and Southeast Asia has contributed to the comparative neglect of fire-related field campaigns in the US [Wiedinmyer et al. 2011]. The Department of Energy Atmospheric Radiation Measurement Climate Research Facility carried out a field campaign (Biomass Burning

Observation Project, BBOP) in 2013 with an instrumented 1-G aircraft from two airfields, i.e., Pasco, Washington (46.24 Lat., -119.10 Long.) and Memphis, Tennessee (35.15 Lat., -90.04 Long.), to address the above-mentioned issues. The Washington observations consisted of wildland (shrub and forest) fires, while the Tennessee site focused on prescribed agricultural (rice and soybean) burns. Among the suite of campaign instrumentation was a filter-based particle/soot absorption photometer (PSAP), which was used to characterize collected aerosol and determine the particle absorption coefficient.

1.1 Particle Absorption by Laser-Heating

A laser-heating approach, referred to as the laser-driven thermal reactor (LDTR) [Presser 2012, Presser et al. 2014], was used to determine the absorptivity of several PSAP glass-fibrous filters, obtained during the BBOP field campaign. Although used in earlier investigations for high-temperature applications, this investigation was carried out at non-reacting, ambient (laboratory) steady-state temperatures. The advantage of using this technique is that 1) absorption is estimated directly from temperature measurements (as opposed to resolving the difference between the measured reflection/scattering and transmission), and avoids the complexities associated with scattering measurements, 2) information is provided for the filter optical properties (while other filter-based techniques empirically remove the contribution of the filter and its effect on absorption), and 3) the analysis considers the presence of the filter material and its effect on particle absorption (e.g., filter material and volatile organics effects on 'absorption enhancement', and particle loading effects leading to 'shadowing' [Presser et al. 2014]). The methodology used for these experiments involves two independent measurements of the sample absorptivity and transmissivity. The absorptivity measurement involves perturbing the temperature of the selected BBOP samples at ambient temperature with a laser beam (probe beam) that impinges directly (normal) onto the filter particle-laden face. When the sample temperature is at the perturbed steady state, the laser beam is blocked and the temperature decay is monitored back to the ambient steady state. Sample absorptivity at ambient temperature and laser wavelength (for this case, in the infrared) was determined using the recorded time-resolved temperatures and a model for thermal energy conservation. Transmissivity measurements, using a traditional arrangement, were carried out independently to provide the particle absorption coefficient. Our earlier investigations (Presser [2012], Presser et al. [2014]) focused on validation of the approach with nigrosin, for which several studies in the literature were available for comparison of results. The objective of this study was to evaluate the LDTR methodology through comparison to measurements from another commercially available instrument, using field campaign filters. To this end, LDTR measurements were carried out with eight sets of PSAP filters (including both blank and particle-laden filters), enabling determination of the isolated-particle (particles only) absorption coefficient and comparison with the PSAP results.

2. EXPERIMENTAL ARRANGEMENT

2.1 PSAP Instrument and Filter Characteristics

The PSAP measures the temporally resolved light absorption coefficient by monitoring the optical transmission through a filter as particles deposit on the filter, using the Beer-Lambert transmission law. The instrument used in the BBOP campaign was a 3-wavelengths light-emitting diode (LED) version (manufactured by Radiance Research, Inc.¹), operating at 462 nm, 523 nm, and 648 nm. The more precise value for each wavelength was measured to be 461.6 nm (21.5 nm), 522.7 nm (38.7 nm), and 648.3 nm (22.9 nm), where the value in parentheses is the respective bandwidth (full width at half maximum) for each line. The instrument references the transmission (i.e., $\tau_j \equiv I_j/I_{j-1} \leq 1$ where j is the index corresponding to the time interval Δt_j) to 1.0 (to remove the filter contribution) and decreases with time as the particle loading increases. A reference filter is used to monitor (and enable correction for) changes in LED emitted intensity, air temperature, and relative humidity with time. Values for the measured air volumetric flow rate, Q_j (for referencing the particle loading on the filter) and computed absorption coefficient are given on a temporal basis. The 'cumulative volume' of particle-laden air passing through the instrument is defined by $V = \sum(Q_j \Delta t_j)$, corresponding to the transmission at $\tau_j = \tau_n$ where n is the sample number. There is a variety of correction schemes used to account for scattering and loading effects that inadvertently increase the absorption coefficient, e.g., Müller et al. [2014], Virkkula [2010], Bond et al. [1999].

The PSAP filters examined for this investigation were Pallflex membrane filters (glass fiber matrix on cellulose paper support fibers bound with vinyl acetate resin), having a diameter of 10 mm and thickness of $114.3 \mu\text{m} \pm 38.1 \mu\text{m}$.² The filter materials and aerosol particles are considered hydrophilic (absorbing water vapor at high relative humidity in clouds), which may contribute to artificially enhancing the filter absorptivity and reducing the transmissivity. The sample air was preheated before reaching the PSAP filter at an estimated temperature of 305 K and relative humidity of 17 %. The PSAP blank filter mass was not measured before exposure to the environment so the captured-particle mass is unknown. The area of the particle-laden portion

¹ Certain commercial equipment or materials are identified in this publication to specify adequately the experimental procedure. Such identification does not imply recommendation or endorsement by the National Institute of Standards and Technology, nor does it imply that the materials or equipment are necessarily the best available for this purpose.

² Estimation of the measurement uncertainty for this study is determined from statistical analysis of a series of replicated measurements (referred to as Type A evaluation of uncertainty), and from means other than statistical analysis (referred to as Type B evaluation of uncertainty) [Taylor and Kuyatt 1994]. The Type A uncertainty is calculated as ku_c , where k is the coverage factor and u_c is the combined standard uncertainty. The value for u_c is estimated statistically by $sn^{-1/2}$, where s is the sample standard deviation and n is the number of samples. For $n = 2, 3, \text{ and } 50$, $k = 4.30, 3.18, \text{ and } 2.01$, respectively, representing a level of confidence of 95 %.

of each filter was measured and estimated to be $(1.964 \pm 0.014) \times 10^{-5} \text{ m}^2$ (the instrument value of $1.783 \times 10^{-5} \text{ m}^2$ was not used for this study [Bond et al. 1999]). The reported total cumulative volume and area of the filter exposed to the collected aerosol were used to provide a characteristic path length (during which time particles impact on the filter) and obtain the total (integrated) transmissivity, absorbance, and absorption coefficient at the three aforementioned wavelengths.

The filters were exposed to atmospheric aerosol during separate BBOP aircraft flights over Memphis, TN (investigating aerosol emissions from agricultural fires). The flight pattern and atmospheric conditions were different for each particle-laden filter, and in general represent sampling of biomass burning aerosol during its early stage of evolution. An example of the flight path and measured absorption coefficient with time are presented in Fig. 1 for the evaluated filter with the heaviest loading (Filter No. 1). The importance of the flight path is to provide a visual of how aerosol ages (i.e., optical properties change with time) from the fire source. Note that the final value for the absorption coefficient at each wavelength is that for the fully coated filter. A Lagrangian sampling strategy was employed in which flight transects orthogonal to the plume direction were conducted at selected distances downwind of the source. This allows one to estimate the time evolution of aerosol properties by moving with the plume such that aerosol in a given transect is derived from the same time and location of the fire. Integrating across transects enhances signal-to-noise at a defined plume age and reduces the uncertainty associated with different instrument response times. The plume age is calculated using prevailing wind speed/direction and the assumption of a constant emission source (i.e., remaining unchanged) during the sampling period.

2.2 LDTR Experimental Arrangement

A detailed description of the LDTR experimental arrangement and operating conditions is given in Presser [2012] and Presser et al. [2014] with an on-line Supplemental Information section. The approach determines the filter absorption with and without the sample particles so as to separate the filter contribution and isolate the optical properties of the aerosol particles. For this investigation, experiments were carried out at the laboratory steady-state temperature and pressure to simulate the condition at which the PSAP instrument operates inside the aircraft. Note that the PSAP uses a cumulative particle approach to coating the filter, while the LDTR is based on analysis of the ensemble of particle coating the filter. Since there is an interest in infrared absorption data [Uzhegov et al. 2005], an available continuous-wave Nd:YAG laser (operating in the infrared at a wavelength of 1064 nm and having a Gaussian intensity profile) was used as the light source for probing the sample filters. Thus, the LDTR was indirectly compared with the PSAP results since the LDTR measurements were carried out in the infrared, while the PSAP provides measurements at three different visible wavelengths. As a result of operating under these conditions, the experimental arrangement was simplified by placing a thermocouple flush with the filter back surface and having the incident laser beam impinge

normal to the filter front surface. In addition to the absorptivity by the LDTR, measurement of the sample transmissivity and a model based on conservation of thermal energy and electromagnetic radiation are required for determining the particle absorption coefficient. It is assumed that the particle-laden filter is represented by an arbitrary homogeneous bulk substance with embedded, more or less uniformly distributed particles [Bohren and Huffman 1983]. Specific modifications to the experiment and measurement protocol from our previous investigations, are described below.

2.2.1 Transmissivity Measurements

A portion of the incident laser beam was diverted for separate transmissivity measurements, as illustrated in Fig. 2. The laser beam diameter was expanded (using a 250 mm focal-length lens) to approximately that of the upstream aperture (completely filling the aperture) that was supported by an aluminum tubular holder (30 mm in length). The BBOP filters (10 mm in diameter) were supported between two apertures (with an aperture diameter of about 7 mm) within the tubular holder. Another aperture (with a 6 mm diameter opening) was placed flush against the face of a power detector (semiconductor photodiode having an active area of 1 cm²) to remove stray light and ensure that all transmitted light passed through the filter. The filter was fixed in position and the analysis did not consider possible variations in the particle loading over the filter face. The detector power meter readings for the incident (without the filter) and transmitted (with the filter) beam intensities were recorded with a personal computer and digital oscilloscope. A neutral density filter (Fig. 2) was used to reduce the laser beam intensity so as not to saturate the detector. Power measurements were repeated twice, recorded, and averaged; the expanded measurement uncertainty was estimated to be better than 1×10^{-5} W. The ratio of the transmitted, I_t , to incident, I_i , intensities provided a measure of the transmissivity (i.e., $\tau \equiv I_t/I_i$) for both the blank and exposed filters. It was assumed that the transmission (and absorption) characteristics of the blank filters were similar to that of the unexposed portion (edge) of the particle-laden filter. There was no workable arrangement to physically support the unexposed portion of the particle-laden filters within the laser beam to obtain the blank-filter transmission (the filter edge being used to support the filter). The transmissivity of the isolated particles (to facilitate comparison with the PSAP results) was determined from $\tau_p = \tau_{ps}/\tau_s$ where p represents the isolated particles, ps is the particle-laden substrate (exposed filter), and s is the substrate (blank filter), see Presser [2012]. It was also assumed that the transmissivity of a particular filter did not change during the LDTR absorptivity measurements at the elevated perturbed temperatures.

2.2.2 Absorptivity Measurements

Absorptivity was measured, based on the arrangement as reported in Presser et al. [2014], but simplified, as illustrated in Fig. 3. The measurement involved centering the backside of the PSAP filter on, and in contact with, a customized K-type fine-wire thermocouple with extensions

(0.25 mm bead diameter, unsheathed, and $0.200 \text{ s} \pm 0.002 \text{ s}$ response time) stationed in the middle of a 5 L vacuum chamber prior to a measurement. We assume that the filter optical properties do not vary spatially, since the laser beam covers the entire particle-laden area of the filter (as with the transmission measurements). The chamber contains five viewing ports (four ports on the chamber side placed 90 degrees apart and one port on the top) for providing optical access. The chamber was used to isolate the environment around the sample from the surrounding ambient. The infrared laser beam was used to perturb the temperature of the PSAP filter, within 10 % of the ambient absolute temperature. The laser power used to perturb the temperature was not observed to alter physically or chemically the particles on the filter. This 'probe' beam can be any laser wavelength (to investigate the measurement wavelength dependency), as long as the sample temperature can be increased and then allowed to decay back to the steady-state temperature. The temperature decay back to the ambient steady-state temperature was then monitored (with a personal computer and data acquisition system) after blocking the probe beam with a beam stop. The rate of change in the sample temperature during the decay portion of the thermogram (i.e., recorded sample temperature with respect to time) was then used to determine the sample absorptivity in the equation for conservation of thermal energy, as described next. Note that these experiments were carried out at ambient (laboratory) conditions (laboratory relative humidity of about 40 % at 298 K), as distinguished from previous experiments [Presser et al. 2014], for which measurements were carried out under reduced pressure and relatively-high temperatures, and requiring a more complex experimental arrangement. Thus, for these experiments, no 'heating' beam or copper sphere were required, greatly simplifying the measurements.

2.2.3 Evaluation for Particle Absorptivity

The following thermal energy balance for bulk substances governs the heating process (excluding the thermal processes associated with chemical reactions):

$$m c_p(T) dT/dt = I_l A \beta(T, \lambda) - F(T, T_o) \quad (1)$$

where the rate of change of sample internal energy is given by the term on the left side of Eq. 1, T is the sample temperature, $c_p(T)$ is the sample specific heat capacity at the sample temperature, and m is the sample total mass. The first term on the right side of the Eq. 1 is the energy absorbed by the sample, where I_l is the laser beam incident radiation intensity that heats the sample, A is the sample geometric cross-sectional area, $\beta(T, \lambda)$ is the sample absorptivity at temperature T and laser wavelength λ . The heat transfer term, $F(T, T_o)$, is defined generically to include arbitrary sample geometries, and represents the sample thermal losses due to conduction through the gaseous medium, substrates, and temperature-sensor wires, and radiation (see Nazarian and Presser [2008]). Convection through the gaseous medium is assumed negligible when operating under vacuum or for small temperature changes (as with the current experiments). The parameter T_o is the sample temperature at steady state, which in this case is

the ambient temperature. The thermal processes (exothermic, endothermic) associated with chemical reaction and vaporization are not considered since the sample mass essentially remained unchanged, and the thermogram profiles do not exhibit unexpected divergences in temperature, for repeated experiments. Thus, one can determine the absorptivity of the blank and particle-laden filters through Eq. 1, using the procedure outlined in Presser [2012], in which the sample temperature is perturbed (within 10 % of the ambient absolute temperature) to another steady-state temperature, T_{max} . Then the laser beam is blocked so that the sample temperature decays back to T_o . Regression fitting of the thermogram (with exponentially decaying functions) at the perturbed steady-state temperature and decay back to the steady-state ambient temperature [Presser 2012] provides values for the temperature-dependent relaxation time, τ^* (representative of the curvature of the regression fit and is used to evaluate dT/dt), T_o , and T_{max} , which then enables one to solve for the heat transfer term and absorptivity $\beta(T, \lambda)$ in Eq. 1.

One can then use conservation of electromagnetic radiation for particle-laden bulk substances to approximate the absorption coefficient of the isolated particles by examining both the blank and particle-laden filters. Determining both β and τ from experimental measurements, the reflectivity, ρ , is derived from the radiation balance equation: $\rho = 1 - \beta - \tau$, and the extinction coefficient is given by [Presser 2012]:

$$\varepsilon = -\frac{1}{d} \ln \left[\frac{\tau}{(1-\rho)^2} \right] \quad (2)$$

where $\tau > 0$, $\rho < 1$, and the characteristic length, d , is defined by the PSAP instrument, i.e., $d = V/A$ where V is the cumulative volume of air passing through the instrument while collecting particles on the filter, and the term A is the cross-sectional area of the filter that was exposed to the particles. Note that ρ is often treated as a surface phenomenon [Incropera and DeWitt 2001], but for fibrous filters it also includes any unobstructed backscattered light past the filter surface from embedded particles/fibers. Thus, when considering the possible contribution of light backscattered from embedded particles/fibers, $\rho \equiv I_p/I_I$ [Presser 2012], where $I_p = I_r + I_{bs}$; I_r represents the reflected light intensity from the filter surface and I_{bs} denotes the unobstructed backscattered light intensity past the filter front surface due to the embedded particles/fibers. Thus, ρ represents all sources of reflected light so as to evaluate correctly ε in Eq. 2.

The extinction coefficient for the isolated particles is $\varepsilon_p = \alpha_p + \sigma_p$, where α_p and σ_p are the isolated particle absorption and scattering coefficients, respectively. It is assumed that the absorptivity and transmissivity of the particle-laden filter are composed of the sum of the individual contributions by the blank filter and isolated particles, and thus are represented by:

$$\beta_{ps} = \beta_p + \beta_s \quad (3)$$

and

$$\tau_{ps} = \tau_p \cdot \tau_s = e^{-A_{ps}^*} = e^{-(A_p^* + A_s^*)} \quad (4)$$

where A^* is the exponent of the transmission law which considers both the absorption and scattering coefficients ($A_i^* = \varepsilon_i d = -\ln(\tau_i)$, $i = p, s, ps$). For the isolated particles case, surface reflection off of the particles is considered negligible (i.e., $\rho_p = 0$ – analysis of the measurements also supports this assumption), and thus $\tau_p + \beta_p = 1$. Particle scattering is also considered in the analysis, however if neglected (as assumed by the PSAP) then $\varepsilon_p = \alpha_p$. Equation 2 then transforms to the same form as used by the PSAP, i.e., $\alpha_p = A/V \ln(1/\tau_p)$. For the blank filter, analysis of the results indicate that surface reflections and absorptivity cannot be neglected (i.e., ρ_s, β_s , and $\alpha_s \neq 0$), and thus ε_s is governed by Eq. 2. For the particle-laden filter case, it can be shown, after substituting Eq. 2 into Eq. 4 for τ_{ps} , τ_p , and τ_s that ε_{ps} will be of the form:

$$\varepsilon_{ps} = \alpha_p + \varepsilon_s + \varepsilon'_{ps} = \alpha_p + \varepsilon_s + \frac{A}{V} \ln \left[\frac{(1-\rho_{ps})^2}{(1-\rho_s)^2} \right] \quad (5)$$

where $\varepsilon_{ps} = \alpha_{ps} + \sigma_{ps}$ and $\rho_{ps} = \rho_s - (1-\tau_p)(1-\tau_s) = \rho_s - \beta_p(\beta_s + \rho_s)$. Note that although the particle loading for the BBOP filters is relatively light, the surface reflectivity for the particle-laden filter is not assumed or found to be the same as the blank filter. If $\tau_p = 1$ (resulting in $\beta_p = \alpha_p = 0$), indicating that there are no particles on the filter surface, then Eq. 5 defaults to the expression for the blank filter (i.e., $\rho_{ps} = \rho_s$, $\tau_{ps} = \tau_s$, and $\varepsilon_{ps} = \varepsilon_s$). If $\rho_{ps} = \tau_p = 0$ (resulting in $\beta_s = \tau_{ps} = 0$), indicating that the particle loading is dense (high particle loading), then $\beta_{ps} = \beta_p = 1$. Substituting the expression for ρ_{ps} into the term ε'_{ps} in Eq. 5, and rearranging terms, results in the following expression:

$$\varepsilon'_{ps} = -\frac{2A}{V} \left[\ln(1 - \rho_s) - \ln[1 - \rho_s + \beta_p(\beta_s + \rho_s)] \right] \quad (6)$$

The above expression indicates that as the particle loading becomes lighter or heavier (as when comparing the different filters of this study), both the particle absorption and filter fiber scattering will affect ε'_{ps} in a nonlinear fashion, and is considered to account for absorption enhancement and shadowing effects.

2.2.4 Measurement Protocol

To evaluate Eq. 1 for the absorptivity, the mass of both the blank and particle-laden filters was measured with an electronic precision mass balance (before and after experiments). As mentioned earlier, there was no observed change in the filter mass after an experiment. The temperature-dependent values for the heat capacity were estimated from the literature for silicon dioxide (quartz fibers, being similar to that of glass fibers) and graphitic carbon (particles) [Haynes 2015-2016], using weight-averaged values as a function of sample temperature. The sample temperature-time derivative and heat transfer terms are determined as described above. The laser power at the position of the sample/thermocouple was measured with a power meter

to be about 85 mW. Along with the transmissivity measurements and aforementioned model, values are determined for the particle absorption coefficient.

Due to the uncertainty associated with the full laser beam alignment/impingement on the filter surface during an experiment and variation in optical properties of each filter, the actual value of laser incident power was estimated during the data analysis. To highly constrain the calculations, several apparent criteria are specified in order to assure the proper determination of the particle extinction coefficient for the isolated particles. Since the value of ε must be positive, the following relationship criteria must be satisfied (see Eq. 2), i.e., $\tau \leq (1 - \rho)^2$ and $\beta \geq \rho (1 - \rho)$. Several additional conditions that must also be satisfied are summarized in Table 1, which relate the particle-laden filter, isolated particles, and blank filter to one another. Also presented in Table 1 are criteria that must be satisfied relating filters with different particle loadings. In general, absorption for the particle-laden filter is required to be larger than the isolated particles, which will be larger than the blank filter ($\beta_{ps} > \beta_p > \beta_s$ and $\alpha_{ps} > \alpha_p > \alpha_s$). Filter surface reflection for the blank filter will be greater than the particle-laden filter, which will be greater than the isolated particles (assumed to be zero) or $\rho_s > \rho_{ps} > (\rho_p \approx 0)$. Transmission for the isolated particles will be greater than the blank filter, which will be greater than the particle-laden filter ($\tau_p > \tau_s > \tau_{ps}$). Similarly, as the filter particle loading increases, relationship criteria must be satisfied to ensure that the absorption properties of heavier loads are greater than lighter loads ($\beta_{ps,h} > \beta_{ps,l} > \beta_s$ and $\alpha_{ps,h} > \alpha_{ps,l} > \alpha_s$), and that transmission and reflection decrease as particle load increases ($\tau_s > \tau_{ps,l} > \tau_{ps,h}$ and $\rho_s > \rho_{ps,l} > \rho_{ps,h}$). Note that if the particles are densely packed together (extremely high particle loading which may lead to shadowing effects), as compared to the filter fiber packing, then the transmissivity criterion may not be satisfied (i.e., $\tau_s > \tau_p > \tau_{ps}$); typically the particle loading is not high on PSAP particle-laden filters to be an issue.

3 RESULTS AND DISCUSSION

3.1 Observed Particle Morphology

Since particle absorption is dependent on its composition, loading, and wavelength of the incident radiation, it is important to provide some discussion regarding the observed physical characteristics of the collected aerosol. Eight sets of PSAP filters were evaluated, with each set including a blank reference filter and a particle-laden filter. The particle-laden filters were ranked according to its observed loading from heaviest to lightest (and referred to as Filter Nos. 1 through 8, respectively). The physical features of the particle-laden filters were observed and recorded using an optical/digital microscope at several magnifications. For the blank filters, the quartz surface appeared to be fibrous, as indicated in Fig. 4A, without any evidence of particle contamination. For the particle-laden filters (see insert in Fig. 4B), particles of varying size and shape (non-spherical and irregular) were randomly dispersed over the exposed portion. Sizes varied from larger dark (absorbing) particles to darkened (blotched) regions of smaller particles (Figs. 4B). Larger pendent particles were detected on the filter fibers that appeared to be nonabsorbing reflective particles (Fig. 4C), while many smaller dark particles adhered to the filter

fibers (Figs. 4D). There was no evidence of the presence of organic carbon coating the filter fibers, as reported by Subramanian et al. [2007].

Secondary-electron-scattered images of the aerosol particles from Filter 4 were acquired of several selected particles (see Fig. 5), using the FEI Nova NanoLab Dual-Beam Field-emission scanning electron microscope, with an electron beam energy at 10 keV and current at 130 pA. The sample size was reduced to an 8 mm diameter disk. Particles (and not filter fibers) were transferred from the sample to a 5 mm x 5 mm polished germanium wafer, using a high-speed, electrostatic-migration micro-centrifugation technique [Conny et al. 2014]. In general, there was a range of aggregated particle sizes and shapes, fairly typical of observed atmospheric aerosols. The smallest spheres (see Fig. 5A), adhering to a larger body, possibly could be soot particles since the sizes are less than 100 nm. They may also appear to be viscous tar balls (i.e., amorphous, spherical, organic aerosol particles with diameters typically between 30 nm and 500 nm). However, the work of Buseck [2016] has shown that the presence of tar balls is primarily associated with wild fires (within the smoke outside the biomass burning plume), while the agricultural burns contain no tar balls but liquid organic matter with larger-size sulfate inclusions. Figure 5B appears to be graphitic carbon due to the plate-like shape of the particle. The irregular-shaped particles in Fig. 5C may be representative of some biological material. The larger aggregates in Figs. 5D were also found to be carbonaceous particles. An x-ray map and spectra were obtained for the particles using an x-ray energy-dispersive-spectroscopy microanalysis system. An example of one particle x-ray spectrum is given in Fig. 5E (for the particle in Fig. 5D), which was obtained from an x-ray map of the particle. The results were similar for all of the examined particles. The x-ray spectra indicate the presence of only carbon and some oxygen (which is attributed to the presence of oxides of the germanium and carbon). The presence of the germanium is attributed to the substrate wafer. The absence of other materials besides carbon for the type of biomass agricultural fires examined in the BBOP campaign indicates that aerosol absorption was purely due to the presence of carbon in the particles.

3.2 Analysis of the Absorptivity/Transmissivity Measurements

Tables 2 presents (as an example) the values used as input parameters for both the blank and particle-laden filters (Table 2A). Values for the input parameters are the average of two repeated measurements. Also presented are analysis results for the optical properties and relationship criteria (of the blank filter, particle-laden filter, and isolated particles) for the sample with the heaviest observed loading (i.e., Filter No. 1). In general, there was some absorption by the fibers of the blank filters in the infrared (for Filter No. 1 the absorptivity was estimated to be about 5.5 % of the incident infrared laser radiation, Table 2B). As reported earlier, this absorption may be attributed, in part, to the hydrophilic behavior of the filter materials, as well as to the cellulose paper backing. All of the relationship criteria were satisfied for this filter (indicative of the positive values listed in Table 2C).

An absorption enhancement factor (α_R) is defined as $\varepsilon_{ps}/\alpha_p$ [Presser et al. 2014], which compares the light extinction coefficient through the particle-laden filter with that of the isolated particles. Enhanced particle absorption due to the presence of the filter is thought to be an artifact of scattering off of the filter fibers, which results in increased particle absorption. Similarly, absorption can be reduced (leading to shadowing) as the particle loading increases to the extent that the incident radiation cannot penetrate the particle field to enable all particles (or filter fibers) to contribute to the absorption process. The particle-laden filter extinction coefficient through the filter is defined by Eq. 5. For an ideal situation in which the particle-laden filter has no absorption enhancement, there will be no particle absorption due to filter fiber scattering (or surface reflections) and the last term in Eq. 5 will be $\varepsilon'_{ps} = 0$ so that $\varepsilon_{ps} = \alpha_p + \varepsilon_s$. Particle absorption will be purely that of the isolated particles and filter fiber scattering (and absorbing if characteristic of the filter material) will be that of the blank filter (without any interaction between the particles and filter fibers). For shadowing, the limiting case would be (as discussed earlier) when the particle loading is such that particles are obscured by higher-layer particles, and thus the lower-layer particles (and filter fibers) do not contribute to the absorption process; then $\varepsilon_{ps} = \alpha_p$. Also, if the particle loading is not so dense and the substrate is completely transparent (no scattering, absorption, or interaction with the particles), then again $\varepsilon_{ps} = \alpha_p$. However, if the particle absorption is influenced by the fiber scattering, then one can represent the modified extinction coefficient as given by Eq. 5.

Equation 5 indicates that the particle-laden filter extinction coefficient ($\varepsilon_{ps} = \alpha_{ps} + \sigma_{ps}$) is dependent on the particle absorption (from α_p), filter fiber absorption and scattering (from $\varepsilon_s = \alpha_s + \sigma_s$), and a more complex term representing the coupling between the particle absorptivity and filter reflectivity. This coupling term can be rewritten as $-2 A/V [\ln(1 - \rho_s) - \ln(1 - \rho_s + \beta_p (\beta_s + \rho_s))]$, being composed of two terms (positive first substrate reflectivity term and negative second term in which the substrate reflectivity is coupled with the sample absorptivity). As indicated in Table 2B, the filter absorptivity β_s (an independent measurement of only the energy absorbed by the filter material) had a value of $\approx 5.5\%$ (ρ_s was $\approx 94.2\%$) of the total incident infrared energy (perhaps attributed to absorbed ambient water vapor in the filter cellulose paper support fibers [Paaso 2007]). Thus ε_s has a relatively insignificant contribution to ε_{ps} , as indicated in Table 2B. The major contributor to ε_{ps} is the coupled term (i.e., comparing the value of ε'_{ps} to the sum of α_p and ε_s), which, as discussed above, represents the enhanced particle absorption in the presence of the filter.

Also noted in Table 2B are higher order reflections off of the filter front and back surfaces, given by the expression $\tau = (1 - \rho)^2 e^{-\varepsilon d} [1 + H.O.T.]$ where $H.O.T. = \rho^2 e^{-2\varepsilon d} + \dots$ [Bohren and Huffman 1983]. As expected, the value for the transmissivity from the first $H.O.T.$ is relatively large for the blank filters (see Table 2B), while the value for the heaviest particle-laden filter is considered negligible since it is significantly less than unity. The value of ε can be determined when including the $H.O.T.$ in the definition of τ for the measured transmissivity unchanged. These modified values of ε ($\varepsilon_{H.O.T.}$) are also presented in Table 2B for the blank filter and heaviest particle-laden filter. The results indicate that the reflections for the blank filter are significant (an order of magnitude increase compared to ε). The contribution of the $H.O.T.$ to the particle-laden filters

is negligible for the heavier coated filters and becomes more significant for the lightest coatings (i.e., with a higher value of reflectivity, resulting in a 11.7 % increase in ε_{ps} for the lightest coated filter). The extinction coefficient for the isolated particles is unaffected because there is no filter, i.e., $\rho_p = 0$.

3.3 Comparison of the LDTR and PSAP Particle Absorption Coefficients

LDTR absorptivity and transmissivity measurements were analyzed for the eight BBOP filters to determine particle absorption coefficient and compare with the PSAP results. Table 3A presents the PSAP cumulative values of the input parameters (for the transmissivity, air flow rate, time, and air volume), and optical properties (absorbance and absorption coefficient at the instrument wavelengths of 462 nm, 523 nm, and 648 nm, Table 3B). In addition, an exponential decaying function (of the form $\tau_p = a_1 + a_2 e^{-a_3 \lambda}$ where a_1 , a_2 , and a_3 are coefficients for the regression fit) was fit to the PSAP transmissivity for each filter at each wavelength and extrapolated to the LDTR wavelength (at 1064 nm) to compare with the separate transmissivity measurements that were carried out for the LDTR analysis. Table 3C presents, as an example, the curve fittings parameters for Filter No. 1, as well as the values for transmissivity and absorbance at each wavelength. In general, the extrapolated transmissivity to 1064 nm matched well with the separate transmissivity measurements, and these values were used in the LDTR analysis for specifying the isolated particle transmissivity.

These results were also compared with absorbance measurements from a scanning, single-beam ultraviolet/visible spectrometer (Perkin Elmer Lambda Bio 20 with a 1053 lines/mm holographic concave grating and 1 nm spectral bandpass) over the wavelength range of 400 nm to 1100 nm. The filters were supported with a mask placed in front of the instrument detector. In a sense, the spectrometer works in a fashion similar to the PSAP in that it zeros out all background information before reporting the particle-only absorbance, and thus information regarding the filter is unavailable (one of the advantages of the LDTR approach). The instrument was zeroed with the blank filter, but this approach did not provide any useful results with particle-laden filter. Therefore, the transmission for the blank filter was obtained separately along with that of the particle-laden filter, and then the two absorbance signatures were subtracted to estimate that for the isolated particles. Because the signal-to-noise ratio was low for the spectrometer absorbance spectra due to the presence of the filter, results are not presented. However, a regression analysis was fit to the data using an exponentially decaying function of the form, i.e., $A^* = a_1 + a_2 e^{a_3 \lambda}$ and the curve compared well with the PSAP and LDTR results. Also, the spectra were broadband (i.e., the mean was relatively featureless over the measured wavelength range), which supported the aforementioned observation that the aerosol particles were essentially carbonaceous.

Table 4 presents a summary of the estimated absorption coefficient results for the eight BBOP filters. The filters are listed according to the observed and measured particle loading from heaviest (No. 1) to the lightest (No. 8). For the PSAP data, the values provided by the instrument

are corrected, as described by Bond et al. [1999]. In general, the correction of the data results in lower values for the absorption coefficient and better match the values obtained for the LDTR (obeying wavelength dependence as given by the Angström power law). The estimated values of the absorption Angström exponent are presented in Table 4 for the two wavelengths 462 nm and 1064 nm (representing the overall range of wavelengths) and also for 462 nm and 648 nm (representing the PSAP range of wavelengths). A scattering correction of 2 % (from nephelometer measurements), as well as other corrections (i.e., particle spot size on the filter, and volume of air drawn through the filter during a measurement), were applied to the PSAP measurements, which resulted in an estimated 2-fold decrease in the corrected particle absorption coefficient. Thus, the scattering correction accounts for about 1 % of the total correction. These corrections modify the PSAP particle absorption coefficient so as to provide a result closer to other non-filter measurement techniques. It does not compare the isolated-particle absorption coefficient to that of the actual particle-laden filter. As expected, the values of the particle absorption coefficient decrease as the observed particle loading decreases. This change is depicted in Fig. 6, which presents the variation of the absorption coefficient with wavelength for the different filters. An exponential decaying function (i.e., $\alpha = a_1 + a_2 e^{-a_3 \lambda}$) is also fit to each data set. Also presented are estimated values for the absorption enhancement parameter, as defined earlier for the LDTR results. This parameter compares the extinction coefficient for the particle-laden and isolated particles. The result provided in Table 4 indicates a 20-fold difference between the particle-laden filter and isolated particles. In general, as the observed particle loading decreases, the value for α_R increases. This result is consistent with the earlier investigation for nigrosin-laden quartz-type filters at ambient temperature (having heavier particle loadings than the PSAP filters of this investigation) [Presser et al. 2014].

For the LDTR absorption enhancement factor, two values are presented in Table 4 for the two lightest filters (Filter Nos. 7 and 8). The first value was determined based on the measured blank and particle-laden filter transmissivity measurements. Using these values, the blank-filter absorptivity becomes larger than that for the isolated particle absorptivity, which violates the criterion $\beta_{ps} > \beta_p > \beta_s$ given in Table 1. However, the order for the particle-laden filter extinction coefficient (from highest to lowest value) is the same as that for the isolated-particle absorption coefficient (as one would expect since the extinction coefficient for all 8 blank filters, having essentially the same optical properties, should and do not vary considerably from filter to filter). Also, the results for the absorption enhancement ratio are in the expected order with reasonable values. One may assume values for the blank and particle-laden filter transmissivity (keeping the isolated particle transmissivity the same), along with the assumed incident laser power, in order to satisfy the above-mentioned criterion of ensuring that the isolated particle absorptivity is greater than that of the blank filter. In this case, one obtains the second set of values for α_R listed in Table 4 for the two lightest-coated filters. These values are much larger than the previous set and not in order. Although the LDTR absorption coefficient (isolated-particles) for these two samples is unchanged from the previous set (see two values listed in Table 4 for Filter Nos. 7 and 8), the values for the blank-filter extinction coefficient (not shown) are unreasonably small, and particle-laden-filter extinction coefficient unreasonably large, as compared to the order of the other 6 filters. In addition, satisfying the above-mentioned criterion results in an assumed

incident laser power larger than the measurement maximum value of 85 mW, and the blank-filter absorptivity is significantly lower (at < 3 %) than the other 6 filters (at 5.2 % to 5.7 %), while expecting the values to be similar. This result indicates that the criterion requiring that $\beta_p > \beta_s$ may not be necessary because although a filter material may have some absorbing component, it is removed through the analysis procedure in determining the isolated particle optical properties. However, it still stands to reason that the absorption properties of the particle-laden filter must be greater than either that of the blank filter or isolated particles.

Conclusions

LDTR absorptivity/transmissivity measurement at ambient (laboratory) conditions were compared with a three-wavelength (visible) PSAP instrument, using PSAP particle-laden filters obtained from the BBOP field campaign. Most likely, the particles coating the filters consisted of soot (having broadband absorption characteristics) and viscous organic material (probably absorbing at shorter wavelengths). The objective of this study was to validate whether the LDTR approach could provide results for particle absorption coefficient that are consistent with other commercially available instrumentation. In general, there was reasonable agreement with the PSAP. One important result of carrying out the LDTR measurements under ambient conditions is that only a thermocouple flush with the filter back surface and the laser beam impinging normal to the filter front surface are required for obtaining the absorptivity, and subsequently the absorption coefficient. In principle, monitoring the filter temperature during and after measurement of the transmissivity (having the laser perturb the sample temperature) can provide a simple approach to obtain both the transmissivity and absorptivity simultaneously [Temple 1985]; as well as the absorption coefficient, using the reported analysis. One can then evaluate the influence of the filter substrate on the particle absorption coefficient. In addition, the analysis was expanded to account for the filter fiber scattering on particle absorption in assessing particle absorption enhancement and shadowing effects.

Acknowledgments

The assistance and helpful comments provided to one of the authors (CP) by Dr. L.C. Brent regarding the PSAP and Dr. P. Chu were much appreciated. The PSAP filters used in this project were provided to NIST by PNNL. The author DC is grateful to Dr. S. Springston (BNL) for the fruitful discussions on PSAP operations. The PNNL and BNL research was supported by the Office of Science of the US Department of Energy (DOE) as part of the Atmospheric Radiation Measurement (ARM) Climate Research Facility and Atmospheric System Research programs. The PNNL is operated by the Battelle Memorial Institute on behalf of DOE under contract DE-A06-76RLO1830. The PSAP data presented in this manuscript are available from the ARM data archive (www.archive.arm.gov) or from the corresponding author. The BBOP would not have been

possible without the contributions by a large number of individuals from PNNL. The BBOP campaign and ARM Aerial Facility were supported by DOE.

Nomenclature

a_1, a_2, a_3	coefficient for regression fitting
A	sample geometric cross-sectional area [m ²]
A^*	exponent of the transmission law
$c_p(T)$	specific heat capacity [J·g ⁻¹ ·K ⁻¹]
d	characteristic path length through the sample (based on the cumulative volume of air passing through the filter in the PSAP instrument) [m]
(dT/dt)	sample temperature derivative [K·s ⁻¹]
$F(T, T_o)$	heat transfer term [W]
I	intensity [W·m ⁻²]
I_I	incident radiation intensity [W·m ⁻²]
I_t	transmitted radiation intensity [W·m ⁻²]
k	coverage factor
L	sample characteristic length [m]
m	sample total mass [g]
n	sample number
P	incident radiation power [W]
Q	volumetric flow rate [m ³ /s]
s	sample standard deviation
t	time [s]
t_c	cumulated time [s]
T	sample temperature [K]
T_{max}	perturbed steady-state sample temperature [K]
T_o	ambient sample temperature [K]
u_c	combined standard uncertainty
V	cumulative volume of air [m ³]

Greek symbols

α	sample absorption coefficient [m ⁻¹]
α_R	enhancement ratio
$\beta(T, \lambda)$	spectral hemispherical absorptivity (fraction absorbed of incident radiation intensity)
Δt	time interval [s]
ΔV	volume of air during Δt [m ³]
ε	sample extinction coefficient [m ⁻¹]
ε'	coupled term due to enhanced particle absorption by the fiber scattering
λ	wavelength [m]
ρ	spectral hemispherical reflectivity (fraction reflected of incident radiation intensity)
σ	sample scattering coefficient [m ⁻¹]

τ	spectral hemispherical transmissivity (fraction transmitted of incident radiation intensity)
τ^*	temperature-dependent relaxation time [s]

Subscripts

<i>abs</i>	absorption measurement
<i>avg</i>	average
<i>bs</i>	backscattered light from embedded particles and filter fibers
<i>cor</i>	corrected
<i>ext</i>	extinction measurement
<i>f</i>	fitted curve
<i>h</i>	higher particle loading on filter
<i>i</i>	index (= <i>p</i> , <i>s</i> , <i>ps</i>)
<i>j</i>	time step
<i>l</i>	lower particle loading on filter
<i>las</i>	laser
<i>n</i>	sample number
<i>p</i>	isolated particles
<i>ps</i>	particle-laden substrate
<i>r</i>	surface reflected light
<i>s</i>	blank substrate

References

- Adachi, K., and Buseck, P.R. (2011). Atmospheric tar balls from biomass burning in Mexico. *J. Geophys. Res. Atmos.*, 116(D5):D05204, doi:10.1029/2010JD015102.
- Andrea, M.O., and Rosenfeld, D. (2008). Aerosol-cloud-precipitation interactions. Part 1. The nature and sources of cloud-active aerosols. *Earth-Sci. Rev.*, 89(1-2):13–41.
- Bohren, C. F., and Huffman, D. R. (1983). *Absorption and scattering of light by small particles*, Wiley, New York, pp. 28–41, 77–81.
- Bond, T.C., Anderson, T.L., and Campbell, D. (1999). Calibration and intercomparison of filter-based measurements of visible light absorption by aerosols. *Aerosol Sci. Technol.*, 30(6):582–600.
- Bond, T.C., Streets, D.G., Yarber, K.F., Nelson, S.M., Woo, J.-H., and Kilmont. Z. (2004). A technology-based global inventory of black and organic carbon emissions from combustion. *J. Geophys. Res. Atmos.*, 109(D14):D14203, doi:10.1029/2003JD003697.
- Burling, I.R., Yokelson, R.J., Akagi, S.K., Urbanski, S.P., Wold, C.E., Griffith, D.W.T., Johnson, T.J., Reardon, J., and Weise, D.R. (2011). Airborne and ground-based measurements of the trace gases and particles emitted by prescribed fires in the United States. *Atmos. Chem. Phys.*, 11(23):12,197–12,216.
- Buseck, P.R. (2016). *Aerosol properties downwind of biomass burns field campaign report*. DOE/SC-ARM-15-076, Dept. of Energy, Office of Science, Office of Biological and Environmental Research, April. <https://www.arm.gov/publications/programdocs/doe-sc-arm-15-076.pdf>
- Chakrabarty, R.K. Moosmüller, H. Chen, L.-W.A. Lewis, K. Arnott, W.P. Mazzoleni, C. Dubey, M.K. Wold, C.E. Hao, W.M. and Kreidenweis S.M. (2010). Brown carbon in tar balls from smoldering biomass combustion. *Atmos. Chem. Phys.*, 10(13):6363–6370.
- Conny, J.M., Collins, S.M., and Herzing, A.A. (2014). Quantitative multiplatform microanalysis of individual heterogeneous atmospheric particles from high-volume air samples. *Anal. Chem.*, 86(19):9709-9716.
- de Gouw, J., and Jimenez, J.J. (2009). Organic aerosols in the Earth's atmosphere. *Environ. Sci. Technol.*, 43(20):7614–7618.
- Goode, J.G., Yokelson, R.J., Ward, D.E., Susott, R.A., Babbitt, R.E., Davies, M.A., and Hao, W.M. (2000). Measurements of excess O₃, CO₂, CO, CH₄, C₂H₄, C₂H₂, HCN, NO, NH₃, HCOOH, CH₃COOH, HCHO, and CH₃OH in 1997 Alaskan biomass burning plumes by airborne Fourier transform infrared spectroscopy (AFTIR). *J. Geophys. Res. Atmos.*, 105(D17):22,147–22,166.
- Environmental Protection Agency (EPA). (2012). *Interagency Monitoring of Protected Visual Environments (IMPROVE) program*. Environmental Protection Agency. <http://www.epa.gov/ttnamti1/visdata.html>.

Haynes, W.M. (Ed.), Handbook of Chemistry and Physics, 96th ed., CRC, Taylor and Francis Group, Florida, 2015–2016, pp. 3-414, 12-205.

Hoffer, A., Gelencsér, A., Guyon, P., Kiss, G., Schmid, O., Frank, G.P., Artaxo, P., and Andreae M.O. (2006). Optical properties of humic-like substances (HULIS) in biomass-burning aerosols. *Atmos. Chem. Phys.*, 6(11), 3563–3570.

Incropera, F.P. and DeWitt, D.P. (2001). *Introduction to Heat Transfer*. 4th edition, Wiley, New York, p. 691.

Jacobson, M.Z. (2012). Investigating cloud absorption effects: Global absorption properties of black carbon, tar balls, and soil dust in clouds and aerosols. *J. Geophys. Res. Atmos.*, 117(D06):D06205, doi:10.1029/2011JD017218.

Kaufman, Y.J., Tanré, D., and Boucher, O. (2002). A satellite view of aerosols in the climate system. *Nature*, 419(6905):215–223.

Kirchstetter, T.W., Novakov, T., and Hobbs, P.V. (2004). Evidence that the spectral dependence of light absorption by aerosols is affected by organic carbon. *J. Geophys. Res. Atmos.*, 109(D21):D21208, doi: 10.1029/2004JD004999.

Kleinman, L.I., and Sedlacek, A.J. (2013). Biomass burning observation project science plan. Department of Energy, Report No. DOE/SC-ARM-13-014.
<http://www.arm.gov/publications/programdocs/doe-sc-arm-15-083.pdf>

Lack, D.A., and Cappa, C.D. (2010). Impact of brown and clear carbon on light absorption enhancement, single scatter albedo and absorption wavelength dependence of black carbon. *Atmos. Chem. Phys.*, 10(9):4207–4220.

Martins, J.V. Artaxo, P. Liousse, C. Reid, J.S. Hobbs, P.V. and Kaufman, Y.J. (1998). Effects of black carbon content, particle size, and mixing on light absorption by aerosols from biomass burning in Brazil. *J. Geophys. Res. Atmos.*, 103(D4):32,041-32,050.

Müller, T. Virkkula, A. and Ogren J.A. (2014). Constrained two-stream algorithm for calculating aerosol light absorption coefficient from the particle soot absorption photometer. *Atmos. Meas. Tech.*, 7(12):4049–4070.

Nazarian, A., and Presser, C. (2008). Thermal and chemical kinetic characterization of multiphase and multicomponent substances by laser heating. *Int. J. Heat Mass Transf.* 51(5–6):1365–1378.

NOAA. (2016). Description of Particle Soot Absorption Photometer (PSAP). National Oceanic and Atmospheric Administration, Earth System Research laboratory, Global Monitoring Division, <http://www.esrl.noaa.gov/gmd/aero/instrumentation/psap.html>.

- Paaso, J. (2007). Moisture depth profiling in paper using near-infrared spectroscopy. VTT Publications 664, academic dissertation, Helsinki, Finland, p. 93. <http://www.vtt.fi/inf/pdf/publications/2007/P664.pdf>.
- Park, R.J., Jacob, D.J., and Logan, J.A. (2007). Fire and biofuel contributions to annual mean aerosol mass concentrations in the United States. *Atmos. Environ.*, 41(35):7389–7400.
- Pósfai, M., Gelencsér, A., Simonics, R., Arató, K., Li, J., Hobbs, P.V., and Buseck, P.R. (2004). Atmospheric tar balls: Particles from biomass and biofuel burning. *J. Geophys. Res. Atmos.*, 109(D06):D06213, doi:10.1029/2003JD004169.
- Presser, C. (2012). Absorption coefficient measurements of particle-laden filters using laser heating: validation with nigrosin. *J. Quant. Spectrosc. Radiat. Transf.*, 113(8):607–623.
- Presser, C., Conny, J.M., and Nazarian, A. (2014). Absorption coefficient measurements of aerosol particle-laden filters using laser heating. *Aerosol Sci. Technol.*, 48(5):515–529.
- Sedlacek III, A.J., Lewis, E.R., Onasch, T.B., Lambe, A.T., and Davidovits P. (2015). Investigation of refractory black carbon-containing particle morphologies using the single-particle soot photometer (SP2). *Aerosol Sci. Technol.*, 49(10):872–885.
- Subramanian, R., Roden, C.A., Boparai, P., and Bond, T.C. (2007). Yellow beads and missing particles: Trouble ahead for filter-based absorption measurements. *Aerosol Sci. Technol.*, 41(6):630–637.
- Taylor, B.N., and Kuyatt, C.E. (1994). Guidelines for evaluating and expressing the uncertainty of NIST measurement results. NIST Technical Note 1297, National Institute of Standards and Technology, Gaithersburg, MD.
- Temple, P.A. (1985). Thin-film absorptance measurements using laser calorimetry, in *Handbook of optical constants of Solids* (Palik, E.D., ed.), Chapter 7, Academic Press, New York, pp. 135–153.
- Tóth, A. Hoffer, A. Nyirő-Kósa, I. Pósfai, M. and Gelencsér, A. (2014). Atmospheric tar balls: aged primary droplets from biomass burning? *Atmos. Chem. Phys.*, 14(13):6669–6675.
- Uzhegov, V.N., Kozlov, V.S., Panchenko, M.V., Pkhalagov, Yu. A., Pol'kin, V.V., Terpugova, S.A., Shmargunov, V.P., and Yausheva, E.P. (2005). Statistical estimation of the atmospheric aerosol absorption coefficient based on the data of optical measurements. Fifteenth ARM Science Team Meeting Proc., Daytona Beach, FL, March 14–18, pp. 1–10.
- Vakkari, V., Kerminen, V.-M., Beukes, J.P., Tiitta, P., van Zyl, P.G., Josipovic, M., Venter, A.D., Jaars, K., Worsnop, D.R., Kulmala, M., and Laakso, L. (2014). Rapid changes in biomass burning aerosols by atmospheric oxidation, *Geophys. Res. Lett.*, 41(7):2644–2651.
- Virkkula, A. (2010). Correction of the calibration of the 3-wavelength particle soot absorption photometer (3 λ PSAP). *Aerosol Sci. Technol.*, 44(8):706–712.

Yokelson, R.J., Goode, J.G., Ward, D.E., Susott, R.A., Babbitt, R.E., Wade, D.D., Bertschi, I., Griffith, D.W.T., and Hao, W.M. (1999). Emissions of formaldehyde, acetic acid, methanol and other trace gases from biomass fires in North Carolina measured by airborne Fourier transform infrared spectroscopy (AFTIR). *J. Geophys. Res. Atmos.*, 104(D23):30,109–30,125.

Wiedinmyer, C., Akagi, S.K., Yokelson, R.J., Emmons, L.K., Al-Saadi, J.A., Orlando, J.J., and Soja, A.J. (2011). The Fire Inventory from NCAR (FINN): a high resolution global model to estimate the emissions from open burning. *Geosci. Model Dev.*, 4(3):625–641, doi:10.5194/gmd-4-625-2011.

Table 1: Various relationship criteria that must be satisfied to assure proper determination of the particle absorption coefficient (dT/dt is the decay temperature-time derivative, τ is the transmissivity, ρ is the reflectivity, β is the absorptivity, and α is the absorption coefficient).

For changing filter case	For changing particle loading
<p>p – isolated particle s – blank filter ps – particle-laden filter</p>	<p>l – lower loading h – higher loading</p>
<p>$dT/dt _{ps} > dT/dt _s$ $\tau_p > \tau_s > \tau_{ps}$ $\rho_s > \rho_{ps} > (\rho_p \approx 0)$ $\beta_{ps} > \beta_p > \beta_s$ $\alpha_{ps} > \alpha_p > \alpha_s$</p>	<p>$dT/dt _{ps,h} > dT/dt _{ps,l} > dT/dt _s$ $\tau_s > \tau_{ps,l} > \tau_{ps,h}$ $\rho_s > \rho_{ps,l} > \rho_{ps,h}$ $\beta_{ps,h} > \beta_{ps,l} > \beta_s$ $\alpha_{ps,h} > \alpha_{ps,l} > \alpha_s$</p>

Table 2: LDTR results for Filter No. 1. Values for the input are the average of two repeated measurements. The subscript *H.O.T.* refers to higher order terms (for reflections off of the filter internal surfaces) for the transmissivity, τ [Bohren and Huffman 1983].

A	Input Parameters		
	Case	Blank filter	Particle-laden filter
$P_{las,abs}$ [mW]		56.50	30.15
m [mg]		2.040 ± 0.001	2.060 ± 0.001
$c_p(T_o)$ [J·g ⁻¹ ·K ⁻¹]		0.770 ± 0.001	0.785 ± 0.001
dT/dt [K·s ⁻¹]		-1.98 ± 0.03	-3.06 ± 0.04
A/V [m ⁻¹]		1.023×10^{-4}	1.023×10^{-4}
T_o [K]		296.8 ± 2.4	297.3 ± 2.4
T_{max} [K]		316.3 ± 2.4	325.6 ± 2.4
τ^* [s]		9.85 ± 0.01	9.26 ± 0.01
$P_{inc,ext}$ [mW]		180 ± 1	180 ± 1
$P_{tra,ext}$ [mW]		0.603 ± 0.010	0.537 ± 0.010

B Optical Properties and Relationship Criteria			
Case	Blank filter	Particle-laden filter	Isolated Particles
τ	0.00335 ± 0.00001	0.00298 ± 0.00001	0.8909 ± 0.0001
β	0.0550 ± 0.0006	0.1640 ± 0.0018	0.1091 ± 0.0019
ρ	0.9417 ± 0.0006	0.8330 ± 0.0018	0.0000 ± 0.0019
$(1-\rho)^2$	0.0034	0.00279	0.9999
$\rho(1-\rho)$	0.0549	0.1391	0.0000
$\tau < (1-\rho)^2$ [$\beta > \rho(1-\rho)$]	0.000054	0.0249	0.1091
<i>First H.O.T. < 1</i> $\epsilon_{H.O.T.}$ [Mm ⁻¹]	8.59×10^{-1} 37.7 ± 0.001	1.01×10^{-2} 229.5 ± 0.001	–
ϵ [Mm ⁻¹] ϵ' [Mm ⁻¹]	1.652 ± 0.001	228.8 ± 0.1 215.3 ± 0.1	11.81 ± 0.01
$\alpha_R = \epsilon_{ps}/\alpha_p$	–	19.36	

C Addition Relationship Criteria							
$\tau_p > \tau_s$	$\tau_s > \tau_{ps}$	$\rho_s > \rho_{ps}$	$\rho_{ps} > \rho_p$	$\beta_{ps} > \beta_p$	$\beta_p > \beta_s$	$\alpha_{ps} > \alpha_p$	$\alpha_p > \alpha_s$
8.876×10^{-1}	4.0×10^{-4}	1.084×10^{-1}	8.33×10^{-1}	5.50×10^{-2}	5.41×10^{-2}	2.17×10^{-4}	1.02×10^{-5}

Table 3: PSAP results for Filter No. 1 (heaviest loading). The given transmissivity, τ , is the value at the cumulated time, t_c [s]. The area of the exposed portion for each filter was estimated to be $(1.964 \pm 0.014) \times 10^{-5} \text{ m}^2$.

A Input Parameters					
τ_{462}	τ_{523}	τ_{648}	Q_{avg} [L·min ⁻¹]	$t_c = \Sigma(\Delta t_j)$ [s]	$V = \Sigma(\Delta V_j)$ [m ³]
7.42×10^{-1}	7.85×10^{-1}	8.38×10^{-1}	1.61	7.26×10^3	1.92×10^{-1}

B Optical Properties					
$\ln(I_i/I_t)_{462}$	$\alpha_{,462}$ [m ⁻¹]	$\ln(I_i/I_t)_{523}$	$\alpha_{,523}$ [m ⁻¹]	$\ln(I_i/I_t)_{648}$	$\alpha_{,648}$ [m ⁻¹]
2.984×10^{-1}	3.052×10^{-5}	2.421×10^{-1}	2.476×10^{-5}	1.767×10^{-1}	1.808×10^{-5}

C Variable	Fitting Parameters for $\tau_p = a_1 + a_2 e^{-a_3 \lambda}$			
	PSAP			LDTR
λ	462 nm	523 nm	648 nm	1064 nm
τ_p	0.742	0.785	0.838	0.891
A^*	0.2984	0.2421	0.1767	0.1155
a_1	0.8978			
a_2	-1.69946			
a_3	0.00518			

Table 4: Estimation of the particle absorption coefficient, absorption Angström exponent, and enhancement factor from the PSAP and LDTR measurements.

Filter No.	Observed Loading	Particle Absorption Coefficient [Mm ⁻¹]				Absorption Angström Exponent	Enhancement Factor
		PSAP [‡]			LDTR [*]		
		$\lambda = 462$ nm	$\lambda = 523$ nm	$\lambda = 648$ nm	$\lambda = 1064$ nm	AAE _{462/1064} / AAE _{462/648}	$\alpha_R = \epsilon_{ps}/\alpha_p$
1	Heaviest	30.53	24.76	18.08	11.81 ± 0.01	1.138/1.549	19.23
2	Lighter	13.89	12.35	10.03	6.53 ± 0.01	0.905/0.962	20.07
3	Lighter	12.19	10.46	8.11	5.62 ± 0.01	0.928/1.205	23.55
4	Lighter	15.87	11.77	7.55	4.91 ± 0.01	1.406/2.196	21.77
5	Lighter	9.67	8.22	6.33	4.74 ± 0.01	0.855/1.252	25.45
6	Lighter	10.70	8.19	5.57	3.99 ± 0.01	1.182/1.930	24.50
7	Lightest	5.11	4.49	3.55	2.41/2.38 ± 0.01 [†]	0.901/1.077	27.23/62.01 [†]
8	Lightest	5.11	4.19	3.04	1.95/1.95 ± 0.01 [†]	1.155/1.535	30.38/46.46 [†]

* Based on the PSAP characteristic length.

‡ The results reported from the PSAP are the corrected values, as stated in Bond et al. [1999]. Estimation of the uncertainty is not available because the transmissivity uncertainty was not provided with the data set. An estimation from the literature [NOAA 2016] is given as about 0.15.

† Satisfying the criterion for $[\beta_{ps} > \beta_s > \beta_p]$ / for $[\beta_{ps} > \beta_p > \beta_s]$.

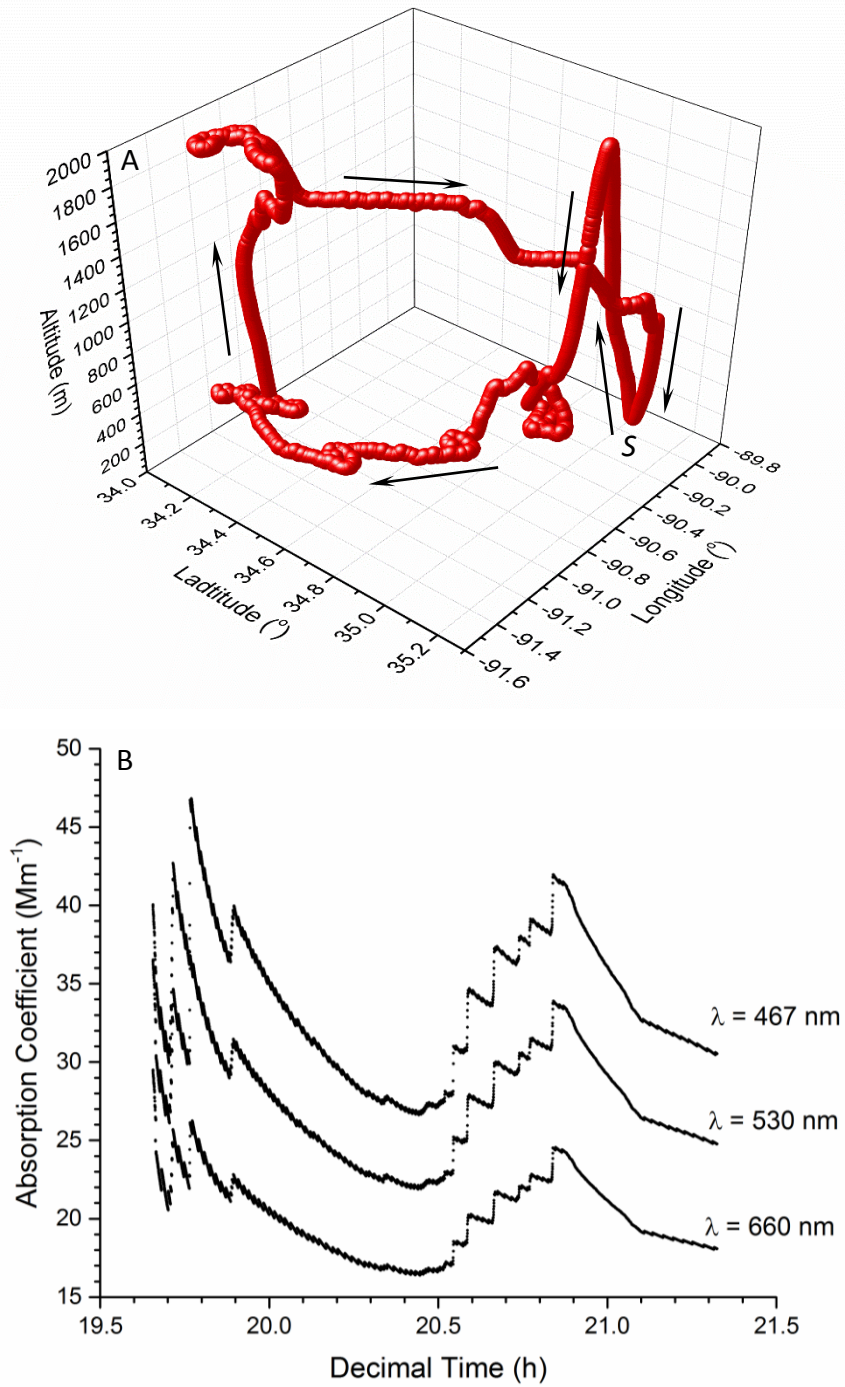


Figure 1. A) Flight path over Memphis, TN for Filter No. 1 (heaviest loading). The 'S' represents initiation of the measurement. B) Variation of the PSAP absorption coefficient with time (decimal value).

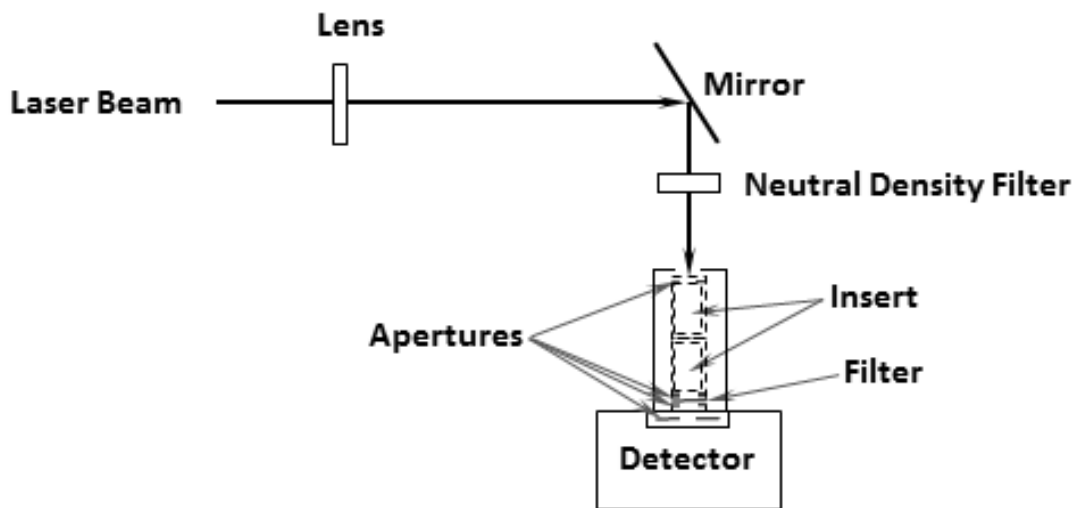


Figure 2. Schematic of the filter transmissivity experimental arrangement.

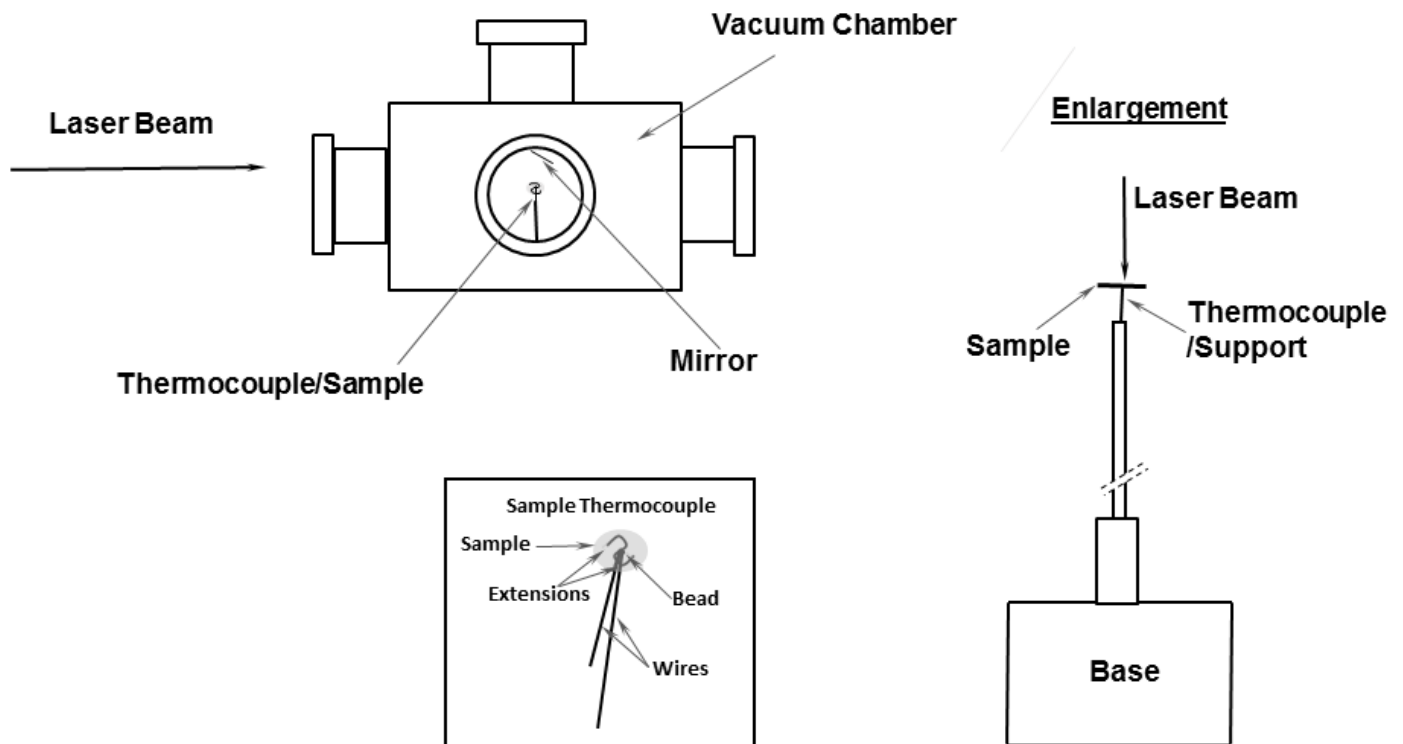


Figure 3. Schematic of the filter absorptivity experimental arrangement.

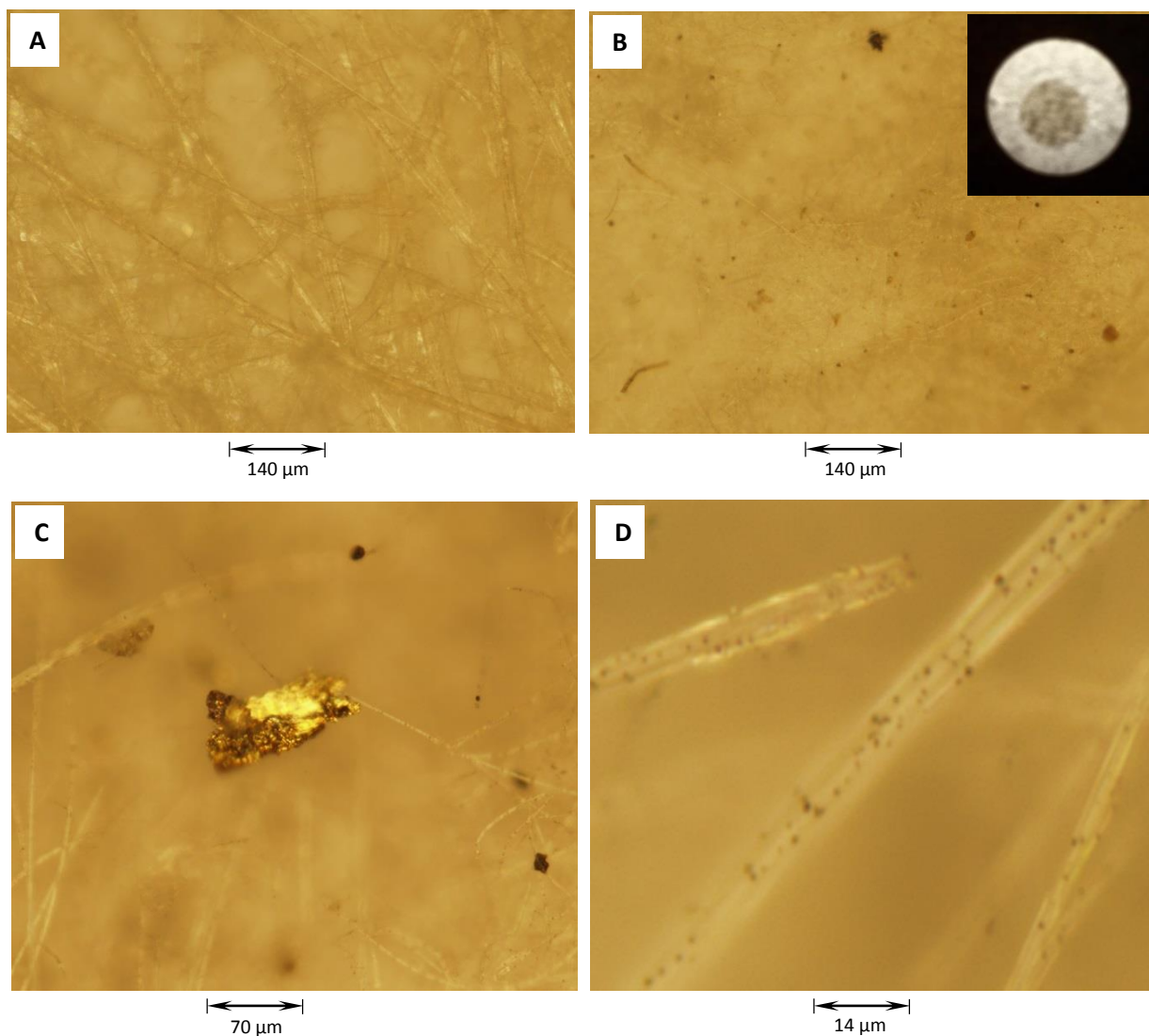


Figure 4. Magnified images of different PSAP filters under a microscope: A) Blank filter ($M = 10$) and B) exposed filter ($M = 10$). M = microscope magnification. Insert is photograph of a particle-laden PSAP filter. Magnified images of a C) larger pendent particle hanging from filter fibers ($M = 20$) and D) smaller particles loading the filter fiber surface ($M = 100$).

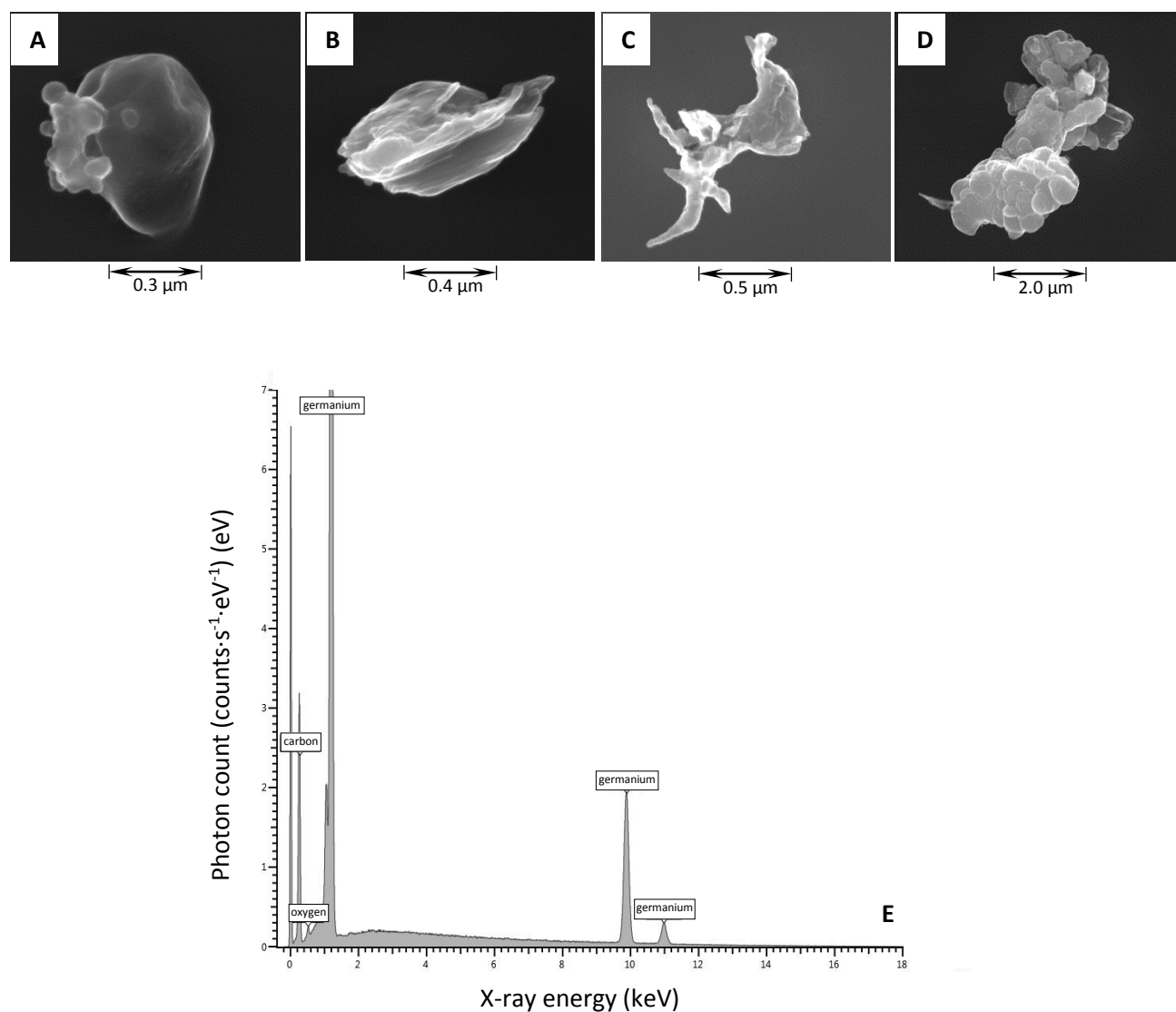


Figure 5. Field-emission scanning electron microscope image of representative particles (for all images: electron beam energy: 10 keV, current: 130 pA, pixel size [nm]: HFW/1024 horizontal pixels (HFW - horizontal field width), secondary-electron mode, and Everhart–Thornley detector). The particle images are arranged in order of decreasing magnification. The magnification (M), and HFW for each respective image are: (A) M: 120 023 x, HFW: 1.07 μm; (B) M: 99 958 x, HFW: 1.28 μm; (C) 50 000 x, HFW: 2.56 μm; (D) M: 20 000 x, HFW: 6.40 μm. Spectra (E) is of a sample particle (Fig. 5D). Sample sits on a germanium substrate. The map was obtained by rastering at 100 μs per pixel for 100 x 112 pixels per frame and averaging 300 frames. The electron beam energy was set at 20 keV and the current at 0.62 nA.

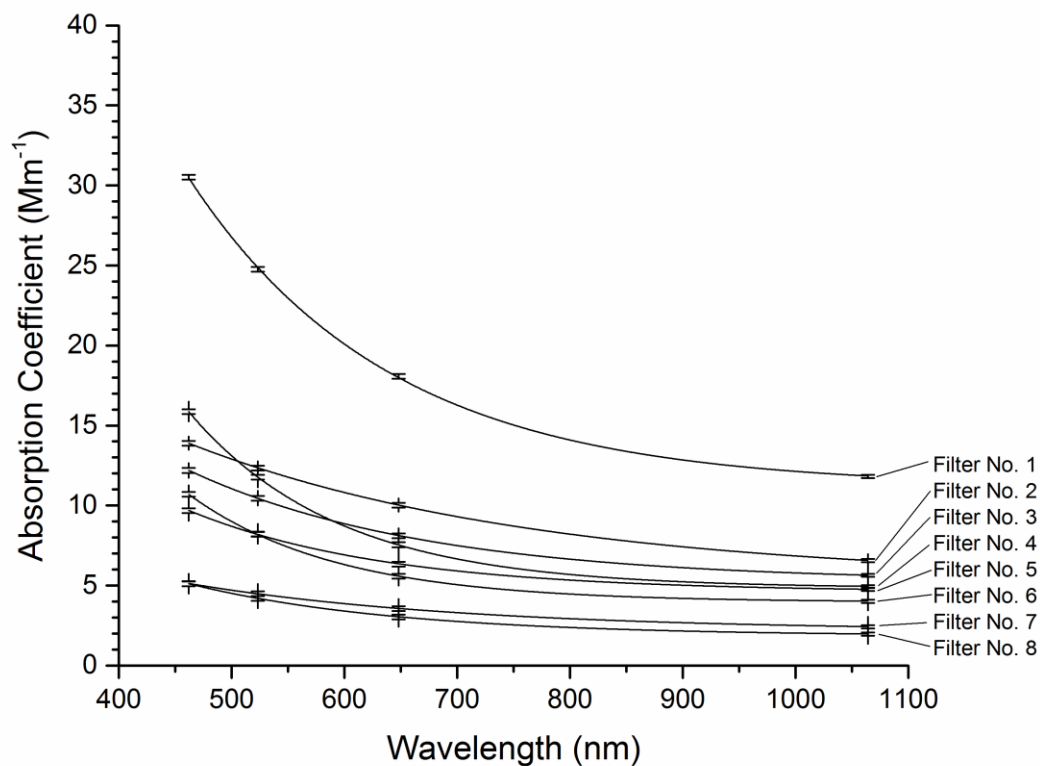


Figure 6. Variation of the absorption coefficient with wavelength for the different PSAP filters (see Table 4). All four data points for each filter are fit to an exponential decaying function of the form: $\alpha = a_1 + a_2 e^{-a_3 \lambda}$, where:

Filter Number	a_1	a_2	a_3
1	1.1174×10^{-5}	2.55821×10^{-4}	0.00559
2	5.33981×10^{-6}	3.81024×10^{-5}	0.00324
3	5.23111×10^{-6}	6.20096×10^{-5}	0.00473
4	4.82094×10^{-6}	3.619×10^{-4}	0.00755
5	4.58941×10^{-6}	7.12791×10^{-5}	0.00571
6	3.9472×10^{-6}	2.3007×10^{-4}	0.00764
7	2.15829×10^{-6}	1.90158×10^{-5}	0.00402
8	1.83572×10^{-6}	3.92953×10^{-5}	0.00538